JOURNAL OF SPACECRAFT AND ROCKETS
Vol. 32, No. 5, September–October 1995

Engineering Notes

ENGINEERING NOTES are short manuscripts describing new developments or important results of a preliminary nature. These Notes cannot exceed 6 manuscript pages and 3 figures; a page of text may be substituted for a figure and vice versa. After informal review by the editors, they may be published within a few months of the date of receipt. Style requirements are the same as for regular contributions (see inside back cover).

Coupled Thermodynamic–Fluid-Dynamic Solution for a Liquid-Hydrogen Tank

G. D. Grayson*
McDonnell Douglas Aerospace,
Huntington Beach, California 92647

Nomenclature

C_v = constant-volume specific heat, $ft^2/s^2 \cdot °R$
g = gravitational constant, ft/s^2
k = thermal conductivity, $slug \cdot ft/s^3 \cdot °R$
β = thermal-expansion coefficient, $°R^{-1}$
μ = dynamic viscosity, slug/(ft/s)
ρ = density, $slug/ft^3$
σ = surface tension, lbf/ft

Introduction

PROPELLANT thermal stratification and fluid-dynamic response to external disturbances are of concern in both launch vehicles and spacecraft. In the past these problems have been addressed separately for want of sufficient computational technology to provide for coupled solutions.[1] This has resulted in overdesigned systems with large safety factors to allow for the uncertainty in modeling techniques. Future systems designed to perform in both high- and low-gravity environments will require less overdesign and safety factors to be technically and financially feasible. Such fluid systems can be based on high-fidelity numerical models only after extensive validation of the models' capabilities in environments where both the thermodynamics and the fluid dynamics are important.

The commercial computer code FLOW-3D[2] has shown promise in both fluid-dynamic and thermal modeling,[1] thus suggesting suitability for solving the coupled mass, momentum, and energy equations in thermodynamic–fluid-dynamic engineering problems. As a first step to achieving a comprehensive solution for complex liquid–gas systems in a launch vehicle, a simple model of a proposed upper-stage liquid-hydrogen (LH_2) tank incorporating the liquid fluid dynamics and thermodynamics is presented here.

FLOW-3D

The FLOW-3D program originated at the Los Alamos Scientific Laboratory and is a derivative of the marker-and-cell method.[3] Extensive code modifications have been made over the years to bring it to its present state.[2] The program is a three-dimensional fluid-dynamic solver that uses a central finite-difference method of numerical approximation to solve the general Navier–Stokes equations. Sections of the momentum and energy equations can be enabled or disabled depending on the particular application. The code provides compressible or incompressible flow assumptions with liquid free surfaces, complex container geometries, several viscosity models, surface tension, flow though porous media, and solidification, to cite a few of the possibilities. Further information on FLOW-3D's capabilities and details of the numerical algorithms can be found in Ref. 2.

LH_2 Tank Model

A 15.3-ft-long, 5.25-ft-radius, cylindrical LH_2 tank with spherical end caps is modeled with FLOW-3D as an axisymmetric tank subdivided by a $28 \times 1 \times 46$ cylindrical-coordinate numerical mesh. Propellant drains from the tank through an 8-in.-diam outlet in the aft end cap at a rate of 7.1 lbm/s during the second-stage engine burn. A 1600-s solution for a typical launch-to-orbit scenario is obtained by FLOW-3D for the upper-stage tank with the following features and numerical approximations:

1) An axial-acceleration model simulating ground hold, first-stage boost, stage separation, second-stage ignition and burn, propellant-settling acceleration, and second-stage engine restart.
2) Separate time-varying, uniform heating rates for the forward end cap, aft end cap, and side wall.
3) A laminar boundary-layer model.
4) Tank draining during second-stage burns.
5) A surface-tension model.
6) A wall-shear model.
7) The liquid density is a function of temperature only.
8) A first-order momentum-equation approximation.
9) No ullage (ullage treated as void region).
10) No heat transfer across the free surface.
11) No phase change.
12) Axial symmetry (negligible lateral accelerations and unsymmetric heating).
13) Constant liquid properties ($\mu, k, C_v, \beta, \sigma$).

Flight Dynamics

A simplified vehicle trajectory model assumes that all lateral accelerations are negligible compared to the axial acceleration. The specified axial-acceleration history represents a launch vehicle with several strap-on solid boosters, a first-stage liquid-propellant booster, and a cryogenic liquid-hydrogen–liquid-oxygen (LO_2) upper stage. The mission is simulated from tank lockup after filling to the second-stage-engine orbital burnout. The time-varying axial acceleration is illustrated in Fig. 1. This acceleration history represents several phases of the mission as summarized below:

1) *Ramp to 1* g (0.0–0.1 s). Initially the vehicle has zero acceleration; then it quickly ramps up to 1 g. A ramp from 0.0 to 32.17 ft/s^2 is used instead of a 1 g impulse to prevent numerical instability.
2) *Ground hold* (0.1–112 s). The tank experiences approximately 2 min of 1 g acceleration. This represents the time on the launch pad after filling between tank lockup and liftoff.
3) *First-stage burn* (112–373 s). The first stage is assumed to have a storable propulsion system with strap-on solid boosters to introduce the maximum dynamic disturbances. The resulting peak acceleration is approximately 130 ft/s^2 (≈ 4 g).
4) *Stage separation* (373–392 s). Low acceleration (2–3 ft/s^2) is followed by 9 s of 10^{-3} g to simulate stage-separation dynamics.
5) *Second-stage burn* (392–883 s). Following stage separation, the second-stage engine fires, yielding an axial acceleration from 15.5 to 36.3 ft/s^2. During this event, hydrogen is drained from the simulated tank at a rate of 7.1 lbm/s.
6) *Settling acceleration* (883–1446 s). At second-stage-engine cutoff, tank draining ceases and a 10^{-5} g propellant-settling acceleration is applied to the vehicle that can be provided by propulsive vapor venting or an external system.

Received Sept. 13, 1994; revision received Jan. 15, 1995; accepted for publication Feb. 17, 1995.

*Engineer/Scientist, Propulsion Analysis and Hydraulics, Space Transportation Division, MS 13-3, 5301 Bolsa Avenue. Member AIAA.

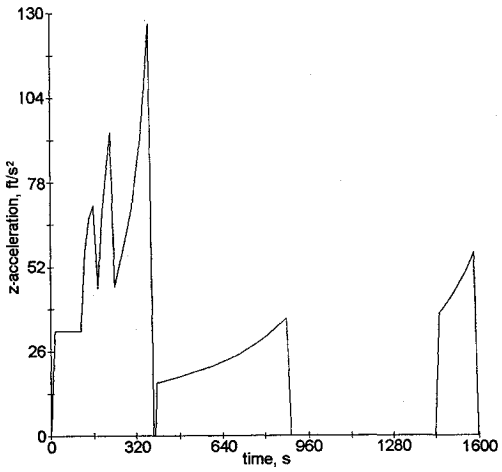

Fig. 1 Axial-acceleration history.

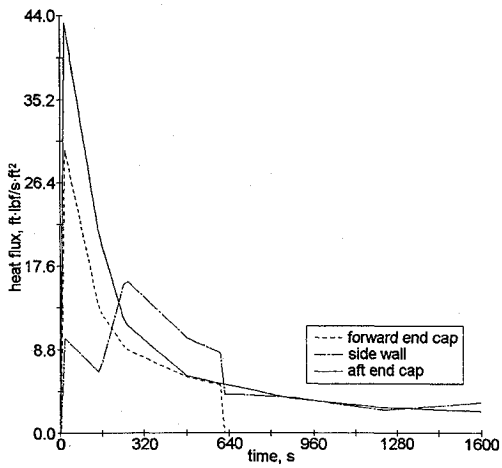

Fig. 2 Heat flux histories.

7) *Second-stage burn* (1446–1596 s). The second-stage engine restarts to circularize the orbit. Propellant draining also restarts, with gravity level varying from 36.9 to 60 ft/s^2.

Tank Heating

The LH_2 tank is heated throughout the entire flight simulation. The thermal environment in a typical upper-stage mission is predicted with an axisymmetric model of the tank using the general heat transfer code SINDA 85. In the FLOW-3D model, tank heating is specified by separate heat flux histories for three segments of the LH_2 tank. Figure 2 illustrates the imposed heating histories for the side wall and the two end caps. The side wall is defined as the cylindrical portion of the tank, and the top and bottom spherical sections represent the forward and aft end caps, respectively.

Results and Discussion

The FLOW-3D calculations were conducted on a Sun Sparc 2 workstation and required approximately 4 days of CPU time. The results of the simulation are described below.

During the ground hold and boost phases, the full tank (97% liquid, 3% ullage gas) is heated while under varying axial acceleration. The initial LH_2 temperature is 37.34°R, which is saturated at 17 psia. As the simulation begins, large temperature (or density) gradients immediately form in the liquid next to all tank surfaces. The gradients create a buoyant flow within the tank where warmer liquid rises (thus moving in the direction opposite the net-acceleration vector) and cooler liquid falls (thus moving in the same direction as the net-acceleration vector). This thermally redistributes the LH_2, feeding the warmest liquid to the upper layers of the propellant. Temperature contours within the liquid are shown in Fig. 3 at 50 s. Large temperature (or density) gradients are indicated by closely packed isothermal surfaces at the side wall and near the aft end cap.

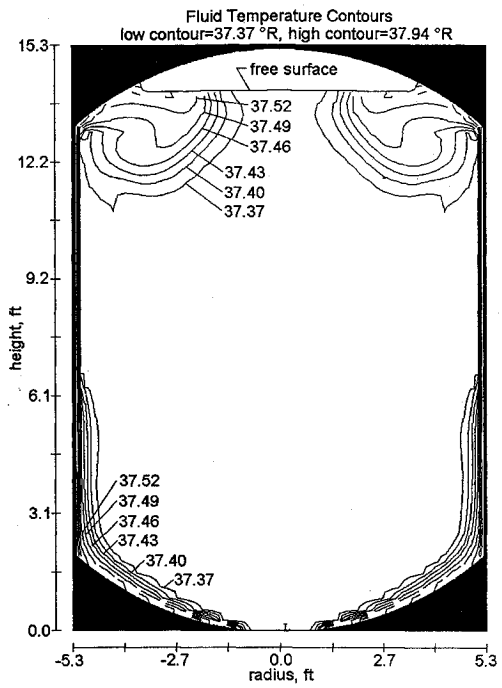

Fig. 3 LH_2 isotherms at 50 s.

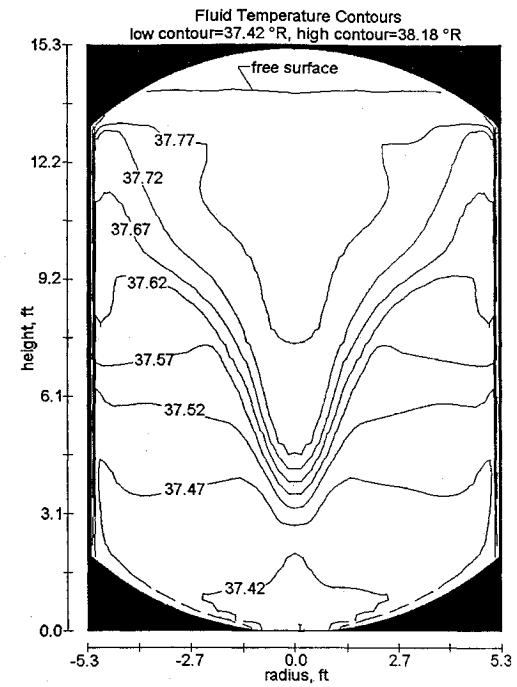

Fig. 4 LH_2 isotherms at 300 s.

A vortex flow at the free surface thermally mixes the propellant at the top of the tank. The temperature distribution shown in Fig. 3 can be explained by considering the buoyant flow field due to heating. An upward motion near the side wall and a vortex flow at the free surface produces the thermal boundary layer near the heated walls and concentric isotherms at the free surface. A slight downward motion at the tank centerline also occurs due to the buoyancy-induced free-surface vortex flow.

After 300 s of heating the liquid has become thermally stratified throughout the tank, with radial and axial variation in temperature as shown in Fig. 4. The downward motion along the tank centerline induced by the free-surface vortex flow tends to pull the fluid isotherms aftward, yielding a radial temperature gradient near the tank centerline. The radial variation is somewhat oscillatory, as the locations of individual isotherms fluctuate during the vehicle boost phase. This oscillation results from dynamic disturbances in the

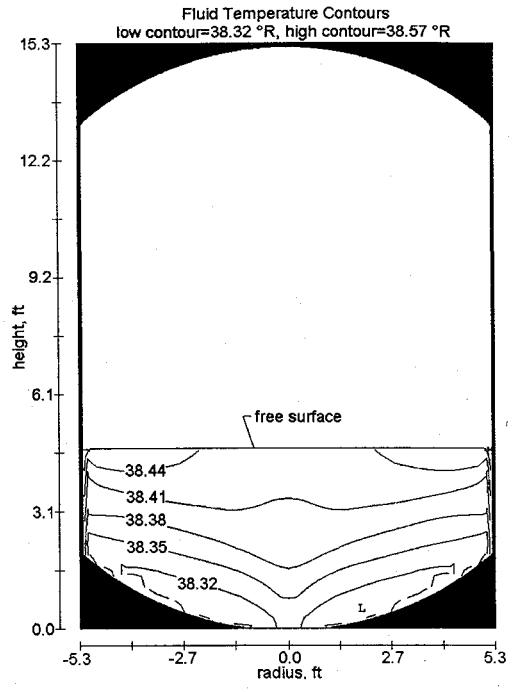

Fig. 5 LH_2 isotherms at 880 s.

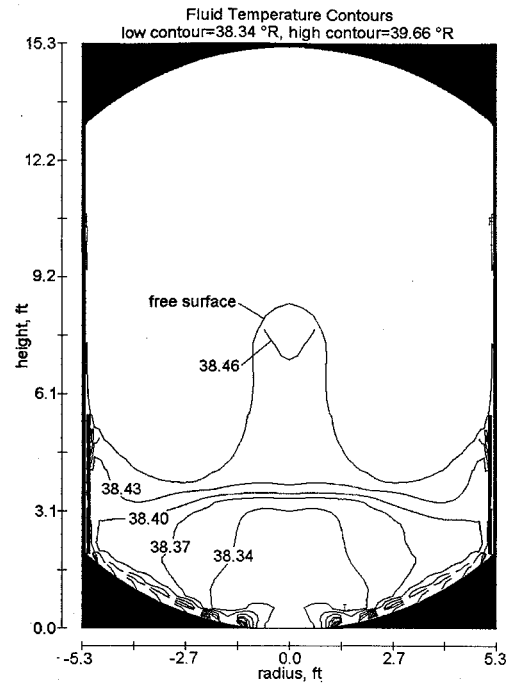

Fig. 6 LH_2 isotherms at 1020 s.

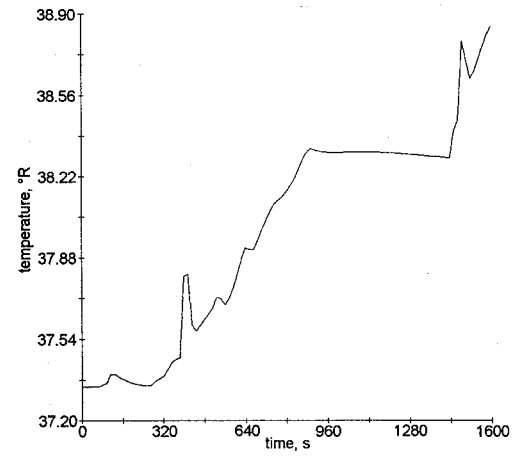

Fig. 7 Tank-outlet temperature history.

mission trajectory such as that from the ejection of the solid strap-on booster engines. The varying acceleration and heating during the first 373 s (ground hold and boost) prevent a steady-state flow. Generally, however, temperature gradients exist near all tank surfaces, and a warmer column of liquid exists along the tank centerline.

The second-stage engine ignition initiates draining of the tank and the liquid continues to stratify. Tank draining initially causes the isotherms to move towards the tank outlet, resulting in a radial temperature variation along the entire length of the tank. During the second-stage burn, relatively warm fluid is drawn into the outlet, with the coldest liquid occupying a toroid-shaped region near the bottom dome. The vortex flow at the free surface is less pronounced once the LH_2 has drained away from the forward end cap. Smaller free-surface vortices mixing the upper layers of the propellant and tank draining both contribute to the recirculating motion within the hydrogen tank.

Prior to engine cutoff, liquid motion within the LH_2 tank is best described as a recirculating flow with downward motion near the tank centerline and upward buoyant flow near the tank side wall. Momentum is imparted to the fluid by buoyancy forces near the tank surfaces while momentum is removed from the system through tank draining. Figure 5 displays the LH_2 isotherms before engine shutdown. Thermal gradients exist near the tank surfaces as well as at the liquid core. A toroid-shaped low-temperature region surrounds the tank outlet, while somewhat warmer liquid is drained. It is noted that the predicted small temperature variations throughout the tank will not affect engine operation significantly. However, inclusion of a phase-change model and three-dimensional heating may increase peak temperatures further, causing even warmer propellant to be ingested. This becomes a critical issue when considering the state of the propellant reaching the pump, where pressures too close to saturation may mean cavitation in at the impeller and the potential for pump damage.

Upon second-stage-engine cutoff at 883 s, tank draining ceases, as does momentum outflow. Axial acceleration decreases from 36.3 ft/s^2 to 0 g in 0.5 s. After 1 s of 0 g, a 10^{-5} g settling acceleration is applied to the vehicle. The buoyant flow within the liquid prior to gravity removal attains a maximum velocity of approximately 1 in./s. In the low-gravity environment, however, normally neglected buoyant velocities became significant and the free surface deforms. Fluid momentum, no longer removed by propellant draining, overcomes the weak settling acceleration, resulting in a thin sheet of liquid moving up the tank side wall and a jet of LH_2 moving upward along the centerline. The slosh wave alters the temperature distribution within the tank as the fluid near the outlet becomes somewhat thermally destratified. A low-temperature area exists directly above the outlet, as shown in Fig. 6. The relatively large axial temperature gradient observed above this cooler liquid region is also a result of the buoyant slosh. After 140 s of low-gravity settling, the slosh wave reverses direction and the propellant begins to return to the aft tank region. The thermodynamic–fluid-dynamic state that generates the above-mentioned behavior is a function of both the temperature effects from heating and the velocity field due to the acceleration environment and draining. Inclusion of advanced models in the Navier–Stokes formulations such as turbulent boundary layers, phase change, and nonaxisymmetric motion and heating will accordingly alter the propellant temperature distribution and low-gravity slosh in the tank.

Prior to engine restart at 1446 s, much of the liquid has returned to the aft region of the tank, but there is still some residual sloshing. The cooler region above the tank outlet shown in Fig. 6 has changed in shape during the low-gravity surface oscillations, yet the outlet temperature has remained approximately constant. Following restart, acceleration increases to 36.9 ft/s^2 and then to 59.6 ft/s^2 in approximately 150 s. This quickly flattens the free surface. During the second burn, the liquid restratifies in a thermal pattern similar to that during the first firing of the second-stage engine shown in Figs. 3–5.

The tank-outlet temperature history is illustrated in Fig. 7. Hydrogen temperature at the outlet fluctuates, but generally increases with

time. The temperature is shown to remain approximately constant during the low-gravity coast. At the restart of the second-stage engine (also the restart of propellant draining), the outlet temperature increases rapidly, indicating that engine reignition results in a rapid thermal restratification.

Conclusions

Numerical modeling methods have advanced to a point where a combined propellant-sloshing and thermal-stratification analysis is technically and financially feasible with existing software and computer hardware. A mission-long solution for a simplified cryogenic upper-stage propellant tank with a highly varying acceleration environment and heating rates presents no significant problems. Results indicate a nonintuitive liquid temperature distribution and slosh due to buoyancy-induced effects in the variable-gravity environment. Even with no propellant slosh, the draining of propellant during engine burn can distort the liquid isothermal surfaces, resulting in earlier ingestion of warmer propellant than would be predicted by a simplified analysis. Although the relatively small temperature variations (<2°R) would not affect engine operation significantly, the resulting low-gravity slosh will affect vehicle control-system requirements.

References

[1]Grayson, G. D., and Navickas, J., "Interaction Between Fluid-Dynamic and Thermodynamic Phenomena in a Cryogenic Upper Stage," AIAA Paper 93-2753, July 1993.

[2]Anon., *FLOW-3D, Computational Modeling Power for Scientists and Engineers*, Technical Manual, Flow Science, Inc., Dec. 1992.

[3]Welch, J. E., "The MAC Method: A Computing Technique for Solving Viscous, Incompressible, Transient Fluid-Flow Problems Involving Free Surfaces," Rept. LA-3425, Los Alamos National Lab., 1966.

T. C. Lin
Associate Editor

Maximum ΔV in the Aerogravity Assist Maneuver

Tomás Elices*
Universidad Politécnica de Madrid, Madrid 28040, Spain

Nomenclature

L/D	= aerodynamic lift-to-drag ratio
r	= pericenter radius, km
V	= velocity of vehicle, km/s
v	= normalized initial velocity at infinity
w	= normalized final velocity at infinity
ΔV	= change in velocity magnitude, km/s
Δv	= normalized change in velocity magnitude
δ	= gravity angular deflection, rad
θ	= arc length in atmosphere, rad
λ	= Lagrange multiplier
μ	= planet's gravitational parameter, km^3/s^2
ϕ	= total rotation angle, rad

Subscripts

c	= circular orbit
max	= maximum value
1	= initial or approach
2	= final or exit
∞	= relative to planet at infinity

Received Jan. 19, 1994; revision received May 18, 1994; accepted for publication May 18, 1994.

*Associate Professor, Department of Aerospace Vehicles.

Introduction

In the last years, a new concept in the field of aero-assisted maneuvers has been developed. This new technique, envisaged for interplanetary missions and named AGA (aero gravity assist),[1,2] utilizes atmospheric flight in order to augment the gravitational bending of heliocentric velocity occurring during a planetary encounter. The resultant ΔV is much larger than that obtained from traditional (exoatmospheric) gravity assist.

This rather paradoxical result (an atmospheric pass, with its inevitable loss of energy, being made to increase the inertial velocity) is illustrated in Fig. 1. The spacecraft enters the planet sphere of influence at the hyperbolic excess velocity following an approach asymptote with pericenter within the atmosphere. The atmospheric flight is controlled by aerodynamic lift to maintain nearly constant altitude. This circular trajectory needs very high values of lift, directed downwards, to counteract the centrifugal force. After the atmospheric turn through an angle, the spacecraft follows the leaving asymptote with a final velocity that, due to drag force, will be smaller than the incoming velocity. It is expected that this reduction will be minimized with appropriate vehicles, such as hypersonic waveriders.[3,4] The triangles of velocities shown at the bottom of the figure demonstrate that, in spite of the reduction in V_∞, the ΔV with such an AGA maneuver is greater than that obtained with gravity assist alone.

It is well known that the maximum ΔV achieved in a gravity assist maneuver is equal to the circular velocity at the hyperbola pericenter. One may ask: given the aerodynamic performance L/D of a vehicle and an approach velocity V_∞, what will be the maximum ΔV in an aerogravity assist maneuver? It is the goal of this Note to give the answer to this question.

Maximum ΔV

The dynamics of an aerogravity assist vehicle can be found in the literature[4] and will not be reviewed here. With the assumption of constant L/D, the final velocity at infinity is

$$V_{\infty 2} = \left[V_{\infty 1}^2 \exp\left\{\frac{-2\theta}{L/D}\right\} + \frac{\mu}{r}\left(\exp\left\{\frac{-2\theta}{L/D}\right\} - 1\right)\right]^{\frac{1}{2}} \tag{1}$$

and the total turning angle

$$\phi = \sin^{-1}\frac{1}{1+r\left(V_{\infty 1}^2/\mu\right)} + \frac{1}{2}\frac{L}{D}\ln\frac{1+r\left(V_{\infty 1}^2/\mu\right)}{1+r\left(V_{\infty 2}^2/\mu\right)} + \sin^{-1}\frac{1}{1+r\left(V_{\infty 2}^2/\mu\right)} \tag{2}$$

is the sum of the gravity turn approach angle δ_1, the arc length θ in the atmosphere, and the gravity turn exit angle δ_2. Since μ/r is the square of the circular velocity at the pericenter, Eqs. (1) and (2) become

$$w = \sqrt{\exp\left\{-\frac{2\theta}{L/D}\right\}(1+v^2) - 1} \tag{3}$$

$$\phi = \sin^{-1}\frac{1}{1+v^2} + \frac{1}{2}\left(\frac{L}{D}\right)\ln\frac{1+v^2}{1+w^2} + \sin^{-1}\frac{1}{1+w^2} \tag{4}$$

where we have introduced the normalized approach and exit hyperbolic excess velocities $v = V_{\infty 1}/V_c$, $w = V_{\infty 2}/V_c$.

The amount of change in heliocentric velocity occurring in an AGA maneuver can be obtained from the corresponding triangle in Fig. 1. After normalizing, we obtain

$$\Delta v = \sqrt{v^2 + w^2 - 2vw\cos\phi} \tag{5}$$

We are interested in achieving the maximum Δv for a given v. In mathematical terms, the problem is formulated as: Find the extreme values of

$$F(w,\phi) = w^2 - 2vw\cos\phi \tag{6}$$